RESEARCH PAPER

China rose petal as biotemplate to produce two-dimensional ceria nanosheets

Junchao Qian · Feng Chen · Xiaobing Zhao ·
Zhigang Chen

Abstract China rose petal was used as robust biotemplate for the facile fabrication of novel ceria nanosheet with a thickness of about 7 nm via a continuous infiltration process. The presence of well-resolved peaks ([111], [200], [220], and [311]) for the products revealed the formation of the fluorite-structured CeO_2. The detailed characterization by field-emission scanning electron microscope (FESEM), field-emission transmission electron microscope (FE-TEM), and atomic force microscopy (AFM) exhibited the biomorphic structure of polycrystalline ceria film with the nanoparticle size of ca. 6.98 nm. Based on the surface chemistry and biochemistry processes, a possible mechanism for the formation of CeO_2 nanosheets is proposed. Furthermore, nitrogen adsorption–desorption measurement and photoluminescence spectrum (PL) were employed to characterize the samples. The ceria nanosheet showed the existence of mesopores (pores 2–4 nm diameter) on its surface and a broad emission ranging from 350 to 500 nm in photoluminescence spectrum. X-ray photoelectron spectroscopy analysis (XPS) confirmed that the mesoporous nanosheets possessed more surface vacancies than the bulk CeO_2; hence these hierarchical CeO_2 layers appear to be potential candidates for catalytic applications.

Abbreviations

2D	Two-dimensional
3D	Three-dimensional
XRD	Powder X-ray diffraction
AFM	Atomic force microscopy
FESEM	Field-emission scanning electron microscope
TEM	Transmission electron microscope
FETEM	Field-emission transmission electron microscope
PL	Photoluminescence spectrum
XPS	X-ray photoelectron spectroscopy

J. Qian · F. Chen · X. Zhao · Z. Chen (✉)
Department of Material Science and Engineering,
Jiangsu University, 212013 Zhenjiang,
People's Republic of China
e-mail: ziyou1900@gmail.com

Introduction

Two-dimensional (2D) anisotropic nanostructures of metal oxides and semiconductor, especially nanosheet with a thickness of several nanometers, have attracted a great deal of attention owing to their unique properties and applications in areas ranging from electronics, separation, and sensor technology to catalysis (Osada et al. 2006; Sugiyama et al. 2010;

Seo et al. 2007). Existing methods for making nanosheets mainly involve hydrothermal synthesis, exfoliation of materials with layered structures, or using surfactant-assisted solution process. But these methods produce only minute quantities of nanosheets (Terrones 2009). Moreover, without intrinsic driving force for 2D anisotropic growth, it is difficult for metal oxides and semiconductors with a cubic crystal structure, including CeO_2, to form nanosheets in solution (Sun et al. 2010).

Ceria is one of the most important rare-earth oxide materials for its promising applications in catalysis, solid oxide fuel cells, oxygen sensors, oxygen storage capacity medium, and chemical mechanical planarization processes (Masson et al. 2009; Sun et al. 2010; Ho et al. 2005). The physical/chemical properties of cerium oxides are strongly dependent on their microstructures, including size, morphology, and specific surface area. The increased nanostructures of ceria lead to increased oxygen vacancies that promote catalytic activity (Liu et al. 2009). However, compared to CeO_2 with three-dimensional (3D) structures such as sphere (Yang et al. 2010) or rods (Tana et al. 2009), 2D nanosheet of ceria has rarely been reported, and therefore the peculiar properties of 2D ceria nanostructure remains to be further explored in more detailed theoretical and experimental studies.

In this study, we report a novel approach to prepare ceria nanosheet via a facile impregnation process with the assistance of a biological template, China rose petal. China rose is perennial flower shrub, within the family Rosaceae. Its petal is composed of specialized, cone-shaped secretory cells and provides a robust, hierarchical layered scaffold whose inner and outer surface can be modified by varying the solution pH. This modification, coupled with its extraordinary chemical and physical stability, makes rose petal an ideal platform for inorganic assembly.

Herein, through a continuous infiltration process of cerium (III) nitrate and subsequent calcination, CeO_2 nanosheets with a thickness of about 7 nm were successfully fabricated. We established a general method by using inexpensive, efficient, and environment-friendly template to synthesize bio-morphic nanomaterial. Based on the surface chemistry and biochemistry interaction, a possible growth mechanism containing metal ions transportation in and out of the cells was proposed and discussed.

Experimental details

Materials

All common laboratory chemicals were purchased from commercial sources and used without further purification. Fresh rose petals were collected from campus in spring.

Pretreatment of China rose petals

Four gram fresh China rose petals were washed with deionized water for several times to remove loose dirt and then pretreated by immersion in ethanol/water mixtures to modify flower cell wall so that the surface could react more easily with cerium(III) nitrate. The reaction was carried out in the Petri dishes (100 mm in diameter). The pH of system was adjusted to 4 by a 5% HCl solution. About 1 h was taken for the above immersion to complete.

Synthesis of ceria nanosheets

2.5 g (Ce $(NO_3)_3$)·$6H_2O$ was added into the resulting mixture and stirred vigorously. The cerium ions infiltrated into petal cell wall at room temperature for 24 h. After soaking, the petals were taken out with tweezers followed by washed with distilled water for several times and dried overnight in an electrical drying oven at 40 °C. Finally, the biotemplate was removed by high temperature calcination (550 °C) for 120 min.

Characterizations

Powder X-ray diffraction (XRD) pattern of the resulting material was obtained by using a D/max-RB powder X-ray diffractometer. The morphology of the sample was observed by using Carl Zeiss Microscope. The surface structure of the samples was further studied by using a Field-emission scanning electron microscope (FESEM) model S-4800.

The distribution of biomorphic ceria nanoparticles was investigated by using a JEM 2100F Field-emission transmission electron microscope (FETEM). The petal-templated hybrid was subjected to thermogravimetric analysis–differential thermal analysis (TGA–DTA) in a SDT Q600 instruments analyzer in an oxygen atmosphere at the heating rate of 2 °C/min.

The adsorption and desorption isotherm study with nitrogen was performed using a Micromeritics ASAP 2010C system. The photoluminescence spectra of samples were measured by using Renishaw In Via laser Raman spectrometer. XPS analysis was carried out by an X-ray photoelectron spectroscopy ESCA (Thermo Fisher Scientific, ESCALAB 250, Mono Al Kα source 1486.6 eV).

Results and discussion

X-ray diffraction

Figure 1 shows a typical XRD pattern of the as-synthesized products after calcination. All of the peaks in this pattern can be indexed as the face-centered cubic fluorite structure of ceria (JCPDS No. 34–0394) and six well-resolved but broad diffraction peaks located at $2\theta = 28.6, 33.1, 47.4, 56.3, 69.5, 76.6$, which could be readily assigned to the fluorite cubic phase (111), (200), (220), (311), (400), and (331) diffraction planes, respectively (Zhou et al. 2005). Peaks arising from impurities are not observed, indicating that protein and carbonaceous materials were completely removed.

Thermogravimetric analysis of hybrid

TGA survey was conducted to investigate the formation of CeO_2 nanosheets during the calcination process. A thermogram of the petal impregnated with cerium
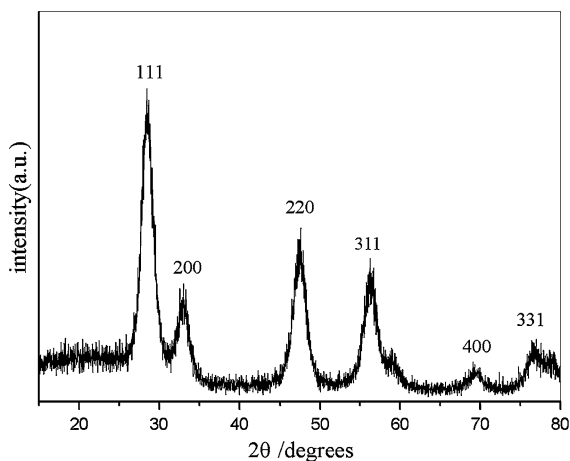
(III) nitrate is shown in Fig. 2. The rate of weight loss almost stopped at 550 °C and the weight loss reached over 85% with petal completely removed due to abundant water in plant cell. Heat flow curve showed two peaks at 281 and 408 °C with an interval about 120 °C, which revealed two-stages in the synthesis of biomorphic CeO_2. It is considered that the weight loss between 200 and 350 °C resulted from the decomposition and charring of the organic constituents. The following weight loss till 550 °C could be assigned to the thorough combustion of those charred products. Therefore, it is suitable for calcination to remove the template at 550 °C (Dong et al. 2006).

The morphology and structure studies

China rose is a bushy, twiggy plant. It is often quite irregular in outline, and ranges in color from deep red to white. After blooming on a flowering stem, the magenta flower petals fully opened as shown in Fig. 3a. Microscopic photograph of the section immersion in water from petal revealed the surface decorated with many irregular lattices (Fig. 3b).

The morphology and structure of the samples is further investigated by field-emission scanning electron microscopy (FESEM). Figure 3c exhibits the right side of original China rose petal pretreated by immersion in HCl/cerium nitrate solution is composed of micro-bowls, like a close-packed array of approximately hemispherical concave surface filled with ridges. The diameters of bowls vary from 8 to 12 μm. As shown in Fig. 3d, the ceria film duplicating the petal's microstructure was obtained by calcining for
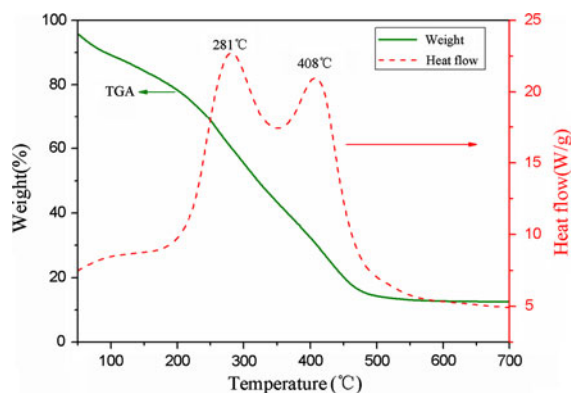

Fig. 1 XRD pattern of cerium oxide nanosheets

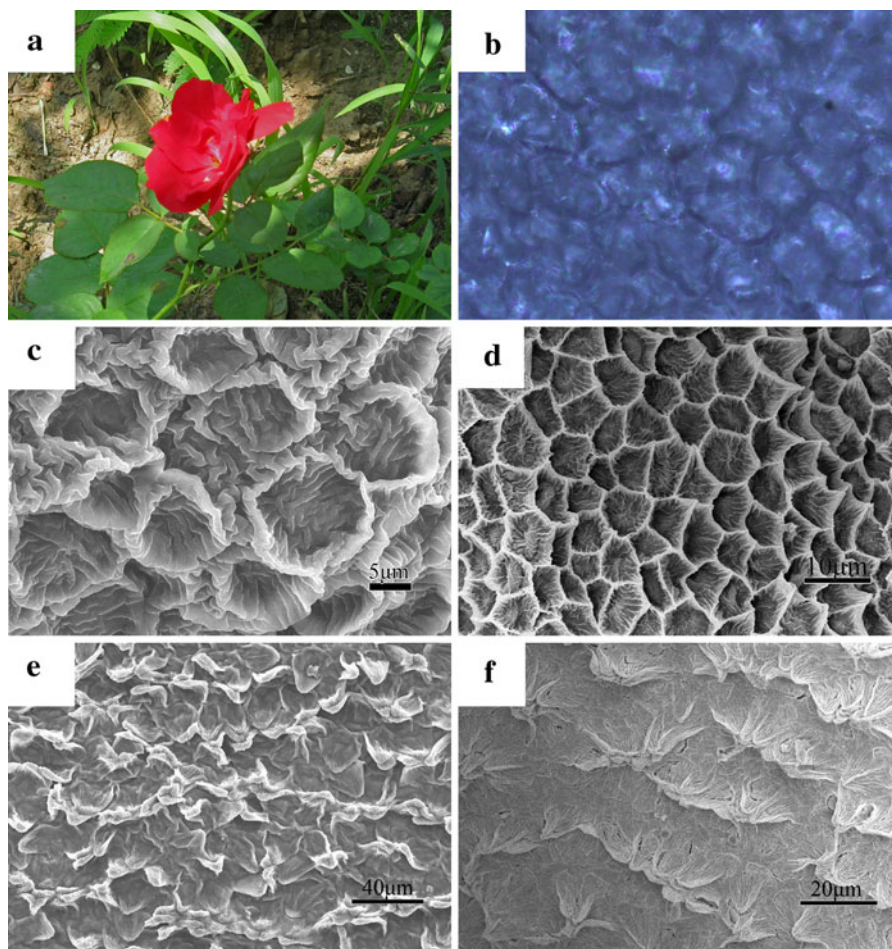**Fig. 2** Thermogravimetric analysis of a mixture of nitrate precursor

Fig. 3 a Photo of China rose. **b** Microscopic observation of original China rose petal, FESEM micrographs of (**c**) the right side of original China rose petal template pretreated by immersion in HCl/cerium nitrate solution (**d**) and **c** after calcined at 550 °C. **e** the reverse side of China rose petal template pretreated by immersion in HCl/cerium nitrate solution (**f**) and **e** after calcined at 550 °C

2 h in air under atmospheric pressure. The surface of the product with a periodic array of embossment shows remarkable microstructure and size similar to that of the original rose petal. The diameter of bowl ranges between 5 and 7.5 μm, owing to shrinkage after high temperature treatment. The same thing goes on at the reverse side of samples. Calcination reduced the rose petal cells with a folding fan structures to about half size (20–10 μm) as seen in Fig. 3e, f. Consequently, the resulting CeO_2 exhibited good replication quality for both micro and nano-sized surface features of the native petal.

Figure 4a, b illustrates the TEM images of CeO_2 synthesized by using petal template after mild sonication. In these regions is the formation of ceria nanosheets as good replicas of hierarchical petal cell wall is evidenced. As shown in the HRTEM images (Fig. 4c), the target material has a polycrystalline phase. Accordingly, the TEM image taken from the edge of ceria nanosheet (Fig. 4b) revealed that the lamellae with a single-layer of polycrystalline nano-particles which had a thickness of approximately 7 nm. HRTEM image in Fig. 4c also displays the distances between the adjacent lattice fringes correspond to the interplanar distances of the cubic CeO_2 (111) and (200), which are $d_{111} = 0.313$ nm and $d_{200} = 0.274$ nm (Yuan et al. 2009). The white circle inserted in picture shows that the length of grain is about 6.98 nm, which conforms to speculation about the thickness of nanosheet in Fig. 4b.

As shown in Fig. 5a, b, the thickness of the nanosheet is calculated to be approximately 7.093 nm. This thickness observed by AFM corresponds to a single CeO_2 polycrystalline particle (6.98 nm) estimated from HRTEM image given above, indicating that the sample was made up of monolayer sheet with the lateral dimension exceeding 150.886 nm.
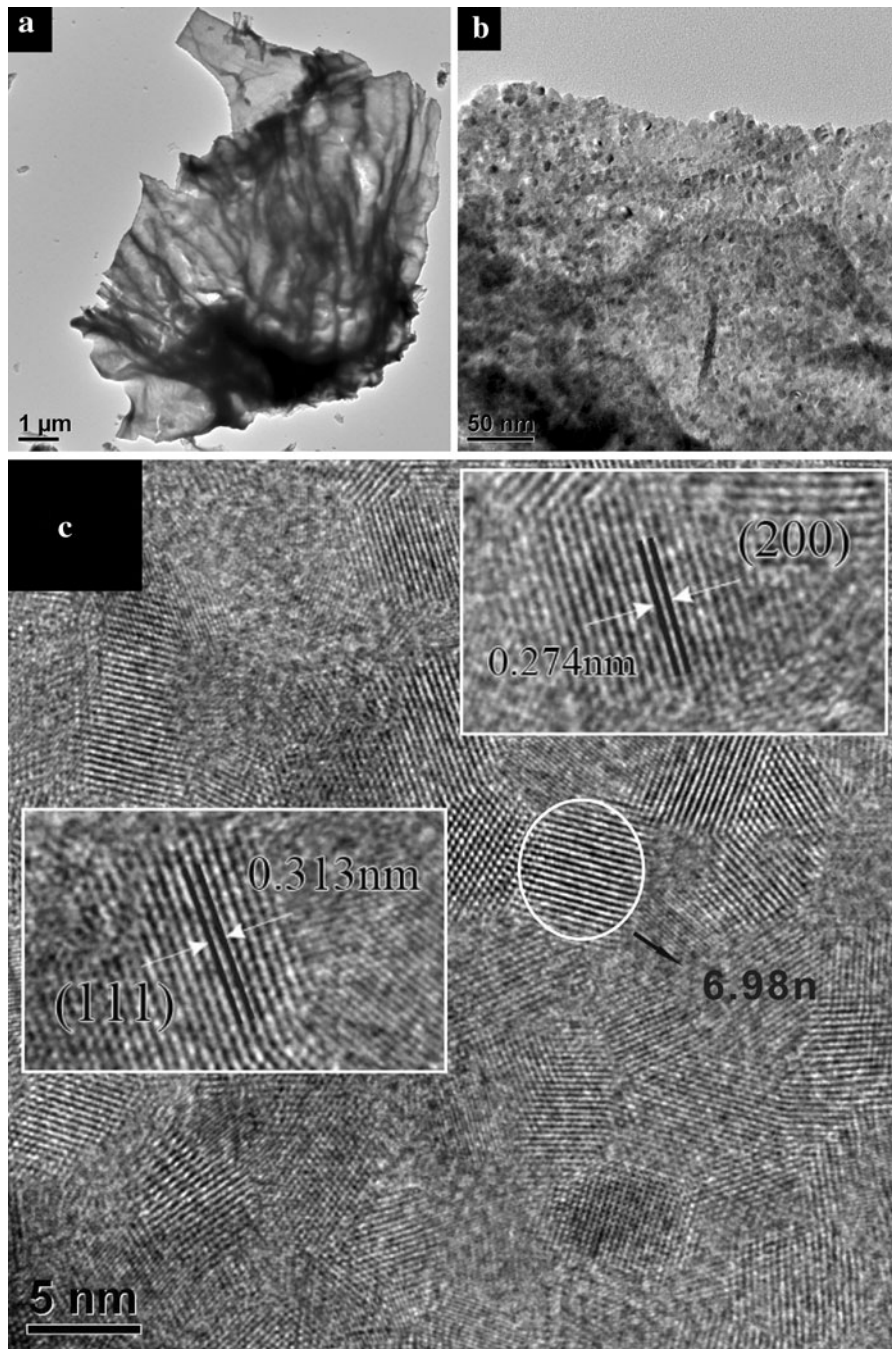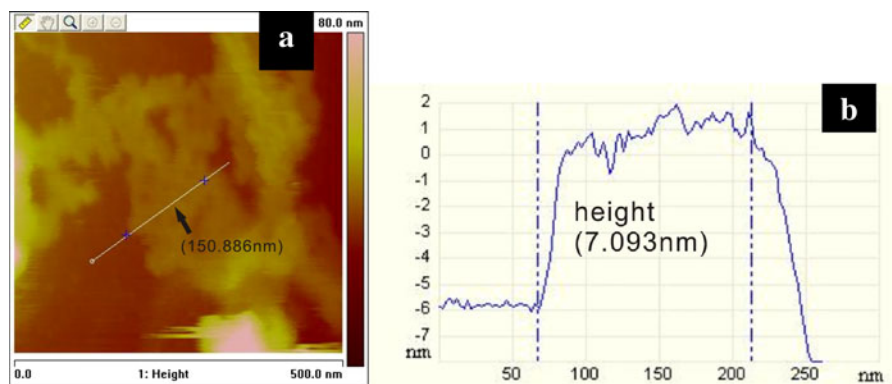

Fig. 4 TEM images of **a** cracked ceria with the morphology of petal cell, **b** the edge of ceria nanosheet, **c** HRTEM image of the CeO_2 nanosheet, insets in (**c**) correspond to the CeO_2 (111) plane (*bottom left*) and the (200) plane (*top right*)

Fig. 5 **a** AFM image and **b** cross-sectional profile of CeO₂ nanosheets deposited on a Si substrate

Proposed mechanism of the formation of CeO₂ using China rose petal as biotemplate

The overall synthetic procedure is depicted in Fig. 6. First, rose petal was treated with deionized water for several times to free from dirt. Figure 6a, b are for a fresh red petal from China rose and an idealized cell model from petals, respectively. Traditional template-directed method always requires several steps to synthesize templates first, which is time-consuming,

high cost (Zhou et al. 2007; Yang et al. 2003). Compared with conventional method, this stage of preparation of biotemplates is more convenient and "environment-friendly".

Mechanisms in biomorphic mineralization can be roughly divided into two types: biologically induced mineralization and biologically controlled mineralization (Hussein et al. 2009). The most likely mechanism involved in the formation of CeO₂ nanosheet is inclined to biologically induced mineralization mechanism
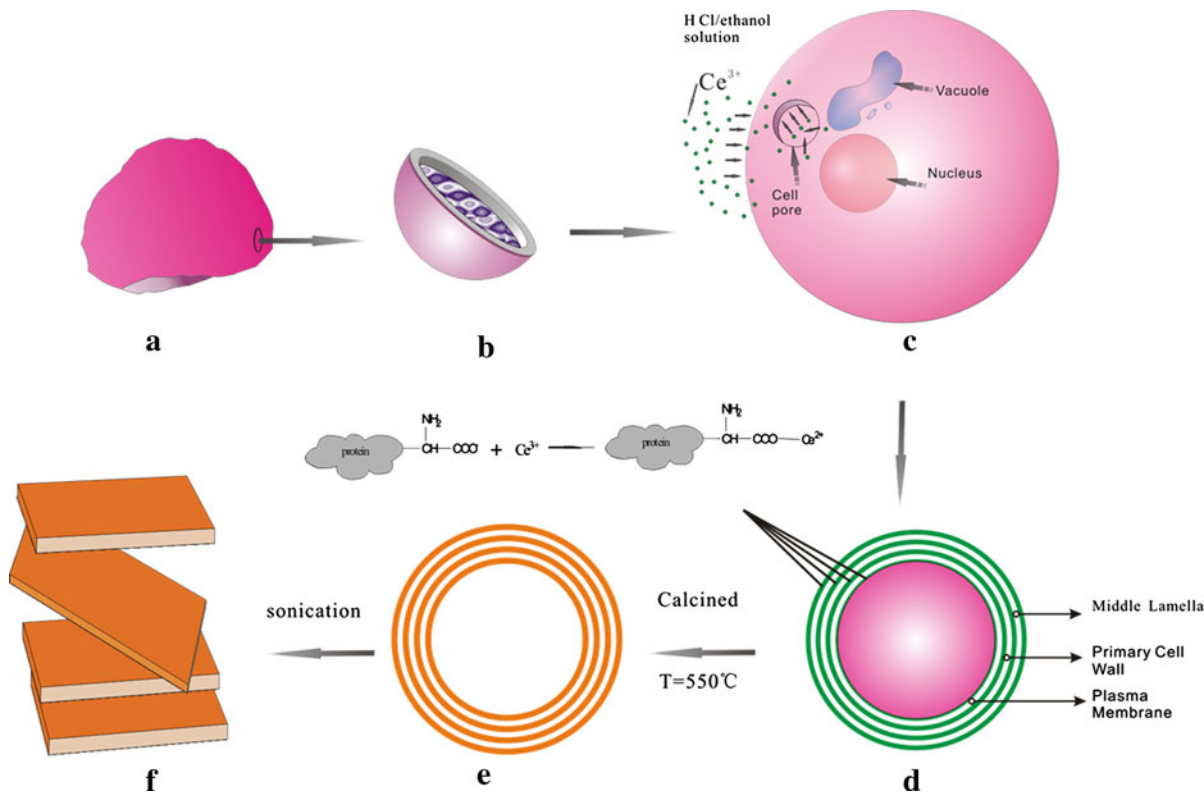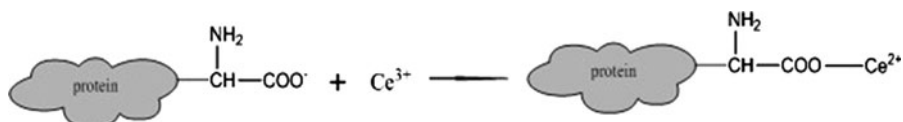

Fig. 6 Schematic illustration of the procedure for the synthesis of ceria nanosheets

which included forming bridges between metal cations and residues within the plant cell wall structure. This point will be illustrated in the next stage in detail.

The second stage consists of two steps, modification of template surface to achieve favorable surface properties and coating the templates with cerium ions. Figure 6c shows the simplified conceptual model of petal cell with a cell pore (magnification) on it. Common plant cell wall mainly contains middle lamella, primary cell wall, plasma membrane, and large amounts of water (Dai et al. 1996; Davies et al. 2002) as shown in Fig. 6c, d. Cerium ions (green dots in Fig. 6c) integrate into petal cell wall through the cell pore to form multi-layers (green circles in Fig. 6d). Anions mainly provided by protein, peptides, and polysaccharides (Lagaert et al. 2009; Hussein et al. 2009) in cell wall are the driving force for assembly to form complexes. Anionic ligand can bind to Ce^{3+} ions, as shown by the exemplar equation below.

Fig. 7a, b. According to the IUPAC classification, the isotherm was identified as type IV with an H4-type hysteresis loop, supporting the mesoporous structure of the material. The presence of a pronounced hysteresis loop in the isotherm curve is associated with the filling and the emptying of the mesopores by capillary condensation. The BET-specific surface area of these ceria nanosheets was measured to be 44.48 m^2/g. The CeO_2 film shows a narrow and bimodal pore-size distribution centered on 2 and 4 nm. These features demonstrate that biomorphic CeO_2 contains large numbers of mesopores (2–4 nm) on the surface of ceria lamellae. Such mesopores could be attributed to duplication of petal cell wall.

Optical properties of ceria nanosheets

PL spectrum is always used to discern defect-related transitions. The location and intensity of some bands

By regulating the cell pores, living cell can hold back the access of metal ions. For this reason, HCl and ethanol were added to cause protein denaturation. Transmission rate of Ce^{3+} ions grew greatly in comparison to reaction without HCl.

Calcination is the final stage to burn off the organic template, as well as to crystallize and densify the products. We choose 550 °C for calcination on the basis of the thermogravimetric analysis and 2 °C/min for heating rate to keep from collapse of nanostructures. Shrinkage occurs subsequent to calcination. As shown in Fig. 6e, bio-membranes in petal cell wall convert to hierarchical CeO_2. After mild sonication, ceria nanosheets, whose lateral size ranges from several hundred square nanometers to several square micrometers, were obtained (Fig. 6f).

Adsorption–desorption isotherm and pore-size distribution

Typical nitrogen adsorption–desorption isotherm and corresponding pore-size distribution are shown in

are related to the oxygen-vacancy density (Sun et al. 2007). The room-temperature PL spectra of bulk CeO_2 powder and the ceria nanosheet are shown in Fig. 8a, b, respectively. (The bulk CeO_2 is obtained by calcining cerium (III) nitrate in air at 600 °C as a contrast.) Compared with the PL spectrum of the ceria nanosheets, the strong room-temperature PL intensity peak at about 600 nm for the bulk CeO_2 could be attributed to its better crystallinity (Sujana et al. 2008).

It is obvious that one strong emission peak band at 425 nm was observed for the nanosheet. Cerium oxide is a wide band gap compound semiconductor, whose gap is about 5.5 eV (Koelling et al. 1983). There are many defects energy levels between Ce 4f and O 2p level. It is easy to observe the hopping from Ce 4f to O 2p. In addition, the defect levels localized between the Ce 4f band and the O 2p band can result in wider emission bands. Thus, the broad emission bands ranging from 350 to 500 nm for nanosheets are attributed to the hopping from different defect levels to O2p band (Lu et al. 2010). This result indicates that the ceria nanosheet possesses higher oxygen-vacancy
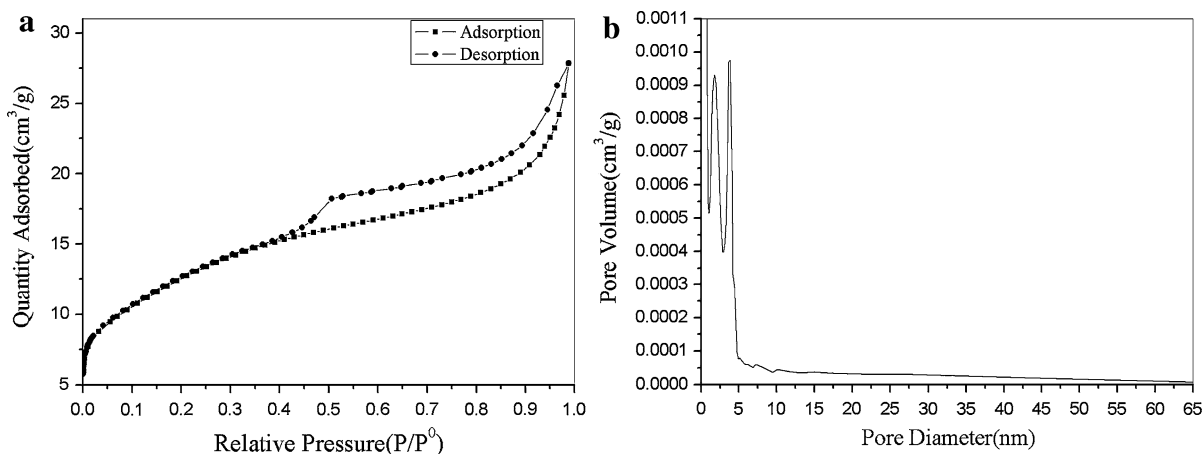
Fig. 7 **a** Nitrogen adsorption–desorption isotherm and **b** corresponding pore-size distribution plot of biomorphic CeO$_2$ nanosheets

level, which is helpful for fast oxygen transport (Sun et al. 2007).

X-ray photoelectron spectroscopy (XPS) analyses

Next we used X-ray diffraction (XRD) analysis to further confirm the result of PL spectra. Figure 9 shows the Ce $3d$ core-level XPS profile for two samples, nanosheet CeO$_2$ and bulk CeO$_2$. Two series of V and U peaks correspond to the $3d_{5/2}$ and $3d_{3/2}$ states, respectively. The peaks of V and V′ can be attributed to a mixing configuration of $3d^9 4f^2(O2p^4)$ and $3d^9 4f^1(O2p^5)$ Ce^{4+} states, and V″ to the $3d^9 4f^0(O2p^6)$ Ce^{4+} state. The valley between V and V′ is attributed to $3d^9 4f^1(O2p^6)$ Ce^{3+} state. The same assignment can be applied to the series of U structures,

and therefore the two valleys between V and V′ and U and U′ are due to photoemission from Ce^{3+} cations. If cerium oxide contains only a small amount of Ce^{3+}, then the valleys are obvious, but if Ce^{3+}/Ce^{4+} ratio in ceria becomes higher, the valleys between V and V′ and U and U′ start to vanish (Ji et al. 2008; Zhang et al. 2004; Noronha et al. 2001; Shyu et al. 1988; Guo et al. 2011). As shown in Fig. 9, the two valleys in XPS spectra of nanosheet is much less well-defined. It is clear that ceria nanosheet has more concentrated Ce^{3+} as well as more oxygen vacancies.

O1 s XPS spectra are shown in Fig. 10. Spectrum 10a from bulk CeO$_2$ surface has two peaks at 527–534 eV. The peak at about 529.74 eV could be attributed to the lattice oxygen (O^{2-}) for CeO$_2$, and the peak at ca. 531.82 eV could be related to the
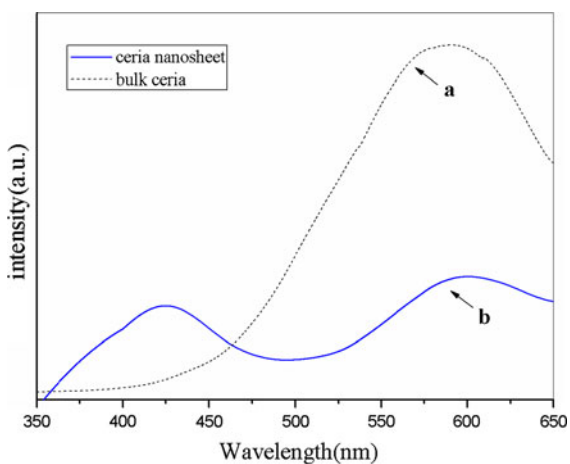

Fig. 8 Room-temperature photoluminescence spectra of **a** bulk CeO$_2$ powder **b** ceria nanosheet
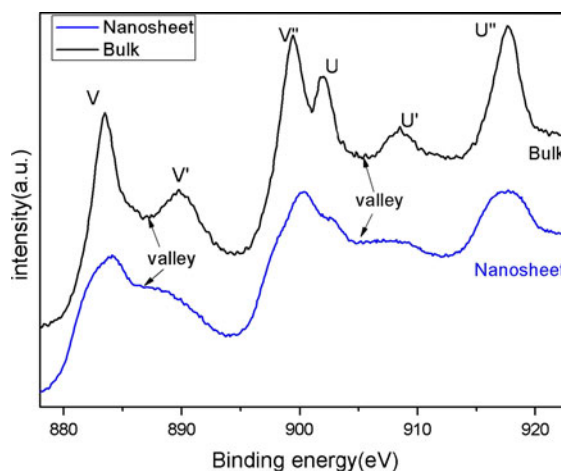

Fig. 9 Ce $3d$ core-level XPS spectra, respectively, for the nanosheet and bulk CeO$_2$
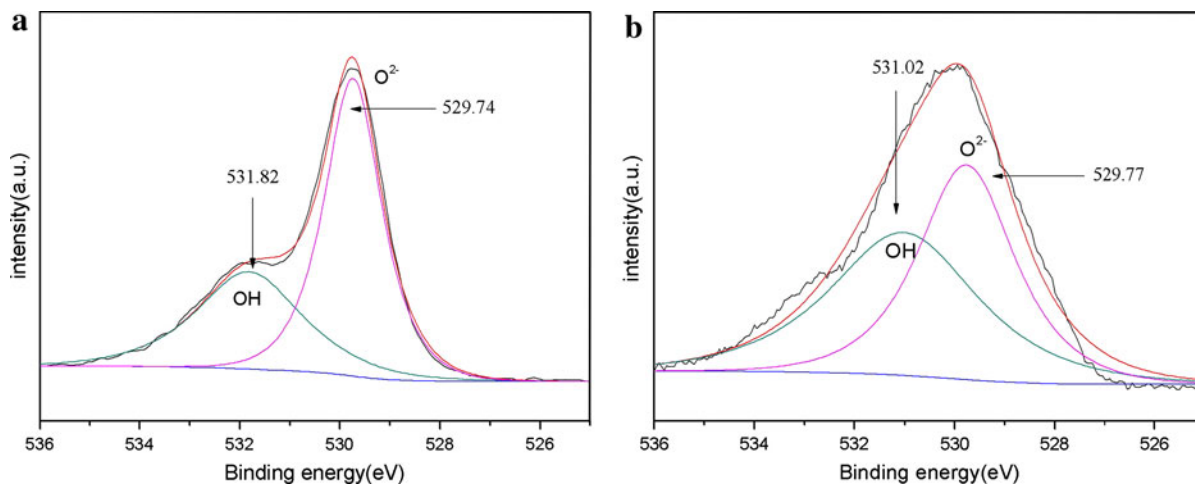
Fig. 10 O 1s core-level photoemission spectra from **a** bulk CeO$_2$, **b** nanosheet

chemisorbed OH on the surface. As shown in Fig. 10b, ceria nanosheet also displays a peak at 531.02 eV belonged to the chemisorbed OH group, which increases appreciably in contrast with the bulk CeO$_2$'s peak. For ceria nanosheet, the percentage of the chemisorbed OH groups out of the total oxygen is significantly larger than that for the bulk. As we know, the increase of Ce^{3+} concentration in nanoparticles correlates with higher oxygen and electron vacancy. It mostly relies on a charge imbalance, the vacancies and unsaturated caused by Ce^{3+}, which could facilitate the growth of chemisorbed oxygen on the catalyst surface (Ji et al. 2008; Liu et al. 2009; Dupin et al. 2000). This indicates the novel CeO$_2$ nanosheet has great potentials as a support for catalysts with various purposes, such as low-temperature water–gas shift reaction and elimination of toxic auto-exhaust gases.

Conclusion

In brief, the synthetic method using China rose petals as a biotemplating agent in this study leads to the formation of novel ceria nanosheets with a thickness of about 7 nm through a simple continuous infiltration process of cerium (III) nitrate. It does not require any intricate treatment or any expensive precursor. The possible growth mechanism of the CeO$_2$ hierarchical architectures was proposed in the light of the electron microscope observation. The synthesis was done based on the surface chemistry, biochemistry processes and interactions between Ce^{3+} with anions aggregated in

the plant cell. In contrast with the bulk CeO$_2$, the as-synthesized biomorphic-CeO$_2$ possesses higher Ce^{3+}/Ce^{4+} ratio and more oxygen vacancies at the surface of the ceria nanosheet, which can be attributed to the quantum size effect associated with its extraordinarily small thickness. This means that catalytic activity of CeO$_2$ nanosheet must be further enhanced. These novel hierarchical porous nanosheets with pore size ranging from 2 to 4 nm and high oxygen-vacancy density strongly suggest their potential application in catalysis.

References

Dai GH, Nicole M, Andary C, Martinez C, Bresson E, Boher B, Daniel JF, Geiger JP (1996) Flavonoids accumulate in cell walls, middle lamellae and callose-rich papillae during an incompatible interaction between *Xanthomonas campestris* pv. malvacearum and cotton. Physiol Mol Plant Pathol 49(5):285–306

Davies LM, Harris PJ, Newman RH (2002) Molecular ordering of cellulose after extraction of polysaccharides from primary cell walls of Arabidopsis thaliana: a solid-state CP/MAS ^{13}C NMR study. Carbohyd Res 337(7):587–593

Dong Q, Su H, Zhang D, Zhu N, Guo X (2006) Biotemplate-directed assembly of porous SnO$_2$ nanoparticles into tubular hierarchical structures. Scr Mater 55(9):799–802

Dupin J-C, Gonbeau D, Vinatier P, Levasseur A (2000) Systematic XPS studies of metal oxides, hydroxides and peroxides. Phys Chem Chem Phys 2(6):1319–1324

Guo M, Lu J, Wu Y, Wang Y, Luo M (2011) UV and visible Raman studies of oxygen vacancies in rare-earth-doped ceria. Langmuir 27(7):3872–3877

Ho C, Yu JC, Kwong T, Mak AC, Lai S (2005) Morphology-controllable synthesis of mesoporous CeO_2 nano- and microstructures. Chem Mater 17(17):4514–4522

Hussein MZ, Azmin WHWN, Mustafa M, Yahaya AH (2009) Bacillus cereus as a biotemplating agent for the synthesis of zinc oxide with raspberry- and plate-like structures. J Inorg Biochem 103(8):1145–1150

Ji P, Zhang J, Chen F, Anpo M (2008) Ordered mesoporous CeO_2 synthesized by nanocasting from cubic Ia3d mesoporous MCM-48 silica: formation, characterization and photocatalytic activity. J Phys Chem C 112(46):17809–17813

Koelling DD, Boring AM, Wood JH (1983) The electronic structure of CeO_2 and PrO_2. Solid State Commun 47(4):227–232

Lagaert S, Beliën T, Volckaert G (2009) Plant cell walls: protecting the barrier from degradation by microbial enzymes. Semin Cell Dev Biol 20(9):1064–1073

Liu X, Zhou K, Wang L, Wang B, Li Y (2009) Oxygen vacancy clusters promoting reducibility and activity of ceria nanorods. J Am Chem Soc 131(9):3140–3141

Lu X-h, Huang X, Xie S-l, Zheng D-z, Liu Z-q, Liang C-l, Tong Y-X (2010) Facile electrochemical synthesis of single crystalline CeO_2 octahedrons and their optical properties. Langmuir 26(10):7569–7573

Masson S, Holliman P, Kalaji M, Kluson P (2009) The production of nanoparticulate ceria using reverse micelle sol gel techniques. J Mater Chem 19(21):3517–3522

Noronha FB, Fendley EC, Soares RR, Alvarez WE, Resasco DE (2001) Correlation between catalytic activity and support reducibility in the CO_2 reforming of methane over Pt/ $Ce_xZr_{1-x}O_2$ catalysts. Chem Eng J 82(1–3):21–31

Osada M, Ebina Y, Takada K, Sasaki T (2006) Gigantic magneto-optical effects in multilayer assemblies of two-dimensional titania nanosheets. Adv Mater 18(3):295–299

Seo J-w, Jun Y-w, Park S-w, Nah H, Moon T, Park B, Kim J-G, Kim Youn J, Cheon J (2007) Two-dimensional nanosheet crystals. Angew Chem Int Ed 46(46):8828–8831

Shyu JZ, Weber WH, Gandhi HS (1988) Surface characterization of alumina-supported ceria. J Phys Chem 92(17):4964–4970

Sugiyama Y, Okamoto H, Mitsuoka T, Morikawa T, Nakanishi K, Ohta T, Nakano H (2010) Synthesis and optical properties of monolayer organosilicon nanosheets. J Am Chem Soc 132(17):5946–5947

Sujana MG, Chattopadyay KK, Anand S (2008) Characterization and optical properties of nano-ceria synthesized by surfactant-mediated precipitation technique in mixed solvent system. Appl Surf Sci 254(22):7405–7409

Sun C, Li H, Chen L (2007) Study of flowerlike CeO_2 microspheres used as catalyst supports for CO oxidation reaction. J Phys Chem Solids 68(9):1785–1790

Sun Z, Zhang H, An G, Yang G, Liu Z (2010) Supercritical CO_2-facilitating large-scale synthesis of CeO_2 nanowires and their application for solvent-free selective hydrogenation of nitroarenes. J Mater Chem 20(10):1947–1952

Tana, Zhang M, Li J, Li H, Li Y, Shen W (2009) Morphology-dependent redox and catalytic properties of CeO_2 nanostructures: nanowires, nanorods and nanoparticles. Catal Today 148(1–2):179–183

Terrones M (2009) Materials science: nanotubes unzipped. Nature 458(7240):845–846

Yang Z, Niu Z, Lu Y, Hu Z, Han CC (2003) Templated synthesis of inorganic hollow spheres with a tunable cavity size onto core-shell gel particles. Angew Chem Int Ed 42(17):1943–1945

Yang Z, Wei J, Yang H, Liu L, Liang H, Yang Y (2010) Mesoporous CeO_2 hollow spheres prepared by Ostwald ripening and their environmental applications. Eur J Inorg Chem 2010(21):3354–3359

Yuan Q, Duan H–H, Li L–L, Sun L-D, Zhang Y-W, Yan C-H (2009) Controlled synthesis and assembly of ceria-based nanomaterials. J Colloid Interface Sci 335(2):151–167

Zhang F, Wang P, Koberstein J, Khalid S, Chan S-W (2004) Cerium oxidation state in ceria nanoparticles studied with X-ray photoelectron spectroscopy and absorption near edge spectroscopy. Surf Sci 563(1–3):74–82

Zhou K, Wang X, Sun X, Peng Q, Li Y (2005) Enhanced catalytic activity of ceria nanorods from well-defined reactive crystal planes. J Catal 229(1):206–212

Zhou H, Fan T, Zhang D (2007) Hydrothermal synthesis of ZnO hollow spheres using spherobacterium as biotemplates. Micropor Mesopor Mat 100(1–3):322–327